Laboratory characterization of silicon avalanche photodiodes (APD) for pulse position modulation (PPM) detection

M. Srinivasan, B. Madden-Woods, J. Hamkins, A. Biswas

Jet Propulsion Laboratory, California Institute of Technology
4800 Oak Grove Dr., Pasadena, CA 91109-8099

ABSTRACT

Two commercially available large area silicon avalanche photodiodes (APD) were characterized in the laboratory. Specifically, the response of the APD's to a sequence of 8-bit pulse position modulated (256-PPM) laser pulses, with and without background noise, was recorded and stored for post analysis. Empirical probability distribution functions (pdf) were constructed from the signal and noise slot data and compared to pdf's predicted by an analytical model based on Webb+Gaussian statistics. The limited pulse sequence was also used to generate bit-error rate (BER) versus signal photons per pulse values, albeit with large error bars. These BER measurements were also compared to results predicted using the Gaussian and Webb+Gaussian models for APD channel statistics. While the measurements qualitatively reflect features predicted by theory, significant quantitative deviations are displayed between the measurements and theory. The source of these discrepancies is not currently well understood, but it is surmised that inaccurate knowledge of detector parameters such as gain and noise equivalent temperature models may explain the discrepancies.

Keywords: avalanche photodiode, pulse position modulation

1. INTRODUCTION

A progress report on laboratory characterization of silicon avalanche photodiodes (APD) is presented. The effort is motivated by the need for developing pulse position modulated (PPM) receivers [1] required for deep space optical communications. The APD is a likely candidate for the front-end opto-electronic conversion device required by the receivers. Previous studies [2] have established that high peak power laser transmitters are required for viable optical links of interest to serve future NASA missions. Consequently, PPM laser transmitters have been identified as the most likely candidates for providing deep space communications needs. Popular wavelengths at which the required peak power can be achieved are the fundamental and second-harmonics of Nd:YAG, Nd:YVO4 and Nd:YLF lasers. As a result, these wavelengths, namely 532 nm and 1064 nm, were chosen for detector characterization. The PPM receivers are being developed to operate in conjunction with large aperture (10m diameter) ground based non-imaging quality telescopes. Therefore the laser signal must traverse an atmospheric path prior to collection and focusing by the telescope. Previous analysis [3] has shown that atmospheric turbulence will limit the achievable focal spot sizes even with a perfect surface quality 10 m telescope to approximately 2 mm in diameter. Furthermore the non-image quality surfaces ("photon bucket") telescopes being considered to reduce cost will only add to the focal spot size. With this in mind, commercially available 3 mm diameter detectors were chosen for characterization.

Photon counting detectors can provide near shot noise limited performance. However, commercially available state-of-the-art photon counting devices do not perform well in the presence of background noise since counts generated due to background noise cannot be distinguished from signal counts, especially when the laser pulse widths are of the order of the detector recovery time (10 to 20 ns). While such detectors may work well for night-time (low background noise) links, their performance will be severely compromised in the presence of background noise. One of the objectives of the present study was to evaluate detectors that would perform in the presence of background noise. This confined the choice of detectors to thermal noise limited devices. Given this limitation the highest achievable quantum efficiency and lowest noise characteristics were sought.

Previous reports on APD detector characterization have usually used a 4-PPM modulation scheme [4]. Moreover, current modulated diode (810-860 nm) [4] and intensity modulated solid state lasers (1064 nm) [5] were used to

The work described was funded by the TMOD Technology Program and performed at the Jet Propulsion Laboratory, California Institute of Technology under contract with the National Aeronautics and Space Administration.

achieve the APD characterization. Sensitivities of 264 incident photons/bit were reported at 1064 nm using such a scheme. In the present work a Q-switched solid sate laser modulated using a 256-PPM scheme (see section 2) with 10-100 kHz repetition rates (compared to the Mbps used previously) is used. The objective of the work was to compare laboratory measurements with an analytical model. Good agreement will allow link design, as well as development of algorithms for symbol and slot synchronization required for developing the back end of the PPM receiver.

2. EXPERIMENTAL SETUP

An Advanced Photonix Model 118-70-74-641 thermoelectrically cooled APD module and a near infrared enhanced EG&G 30659G APD integrated to a custom high voltage temperature controlled (HVTC) board supplied with the APD, were used at 532 and 1064-nm. Fig. 1 shows a schematic representation of the experimental arrangement used. A Q-switched Nd:YVO4 laser oscillator [6] is used to provide 1064 nm light with a pulse width that varies from 1.9 - 3 ns for repetition rates of 1 - 100 kHz. When 532 nm light was being used for detector characterization the 1064 nm light was transmitted through a focusing lens and a lithium niobate crystal frequency doubler assembly shown enclosed in the dashed box in Fig. 1. The collimated laser beam at 1064 or 532 nm was incident through a variable attenuator and pellicle beam splitter on a lens that focused the light down to a spot. The light path following the lens was split by a second pellicle beam splitter so that it was simultaneously incident upon a power sensor (Anritsu Model) and the APD to be characterized. The splitting ratio of the 532 and 1046 nm light was calibrated separately by moving the power sensor back and forth between the two locations.

The pellicle beam splitter preceding the lens in the light path allowed the introduction of background white light from a tungsten source emitting through a light pipe. The white light was filtered using a narrow band pass filter (10 nm @ 532 and 3 nm @ 1064 nm). The split in the white light power was also separately calibrated.

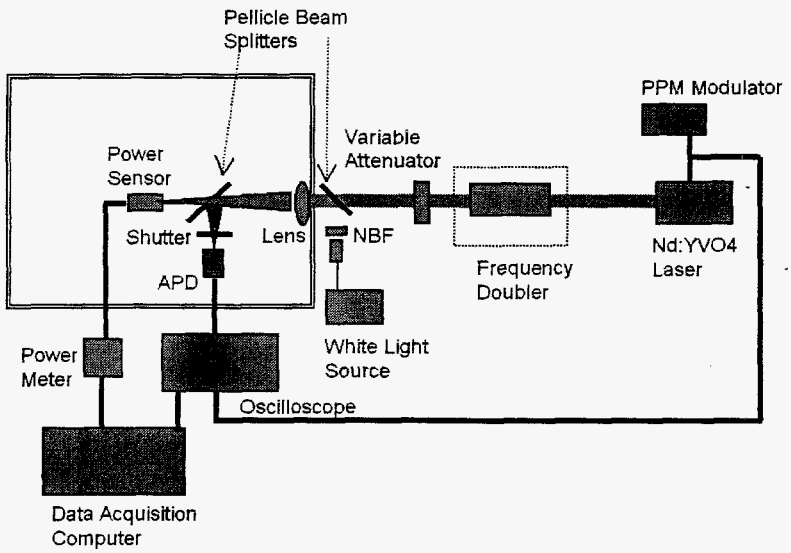

Figure 1. A schematic layout of the experimental arrangement used for performing the detector characterization

The laser is externally modulated using the PPM modulator which consists of an electronic timing circuit that can simulate a restricted version of 256-PPM in which the pulses are stepped sequentially through the 256 slots using a ring counter. The slot width can be independently varied at the chosen pulse rate. In the results to be presented, 50 kHz and 100-kHz repetition rates with 25 ns (532 nm) and 10 ns (1064 nm) slot widths were used.

The power sensor, APD, and lens assembly were enclosed inside a light tight box with a hole to admit the laser and white light. An electronic shutter operated remotely from outside the enclosure (not shown in figure) allows blocking of the APD.

The procedure followed for acquisition of PPM data consisted of attenuating the laser beam to arbitrary low average powers so that barely a few pulses were sensed by the APD. A data stream was recorded for post analysis. The attenuation was gradually reduced while pulse sequences were recorded. The low average powers used were

usually below the -65 dBm sensitivity level of the power sensor; however, by using the remotely operated electronic shutter, the detector could be blocked and the power recorded without attenuation, while making a note of the repeatedly calibrated attenuation used. This was found to be the most reliable method of determining the average incident power from which the average photons per pulse could be determined.

A Tektronix 754C oscilloscope was used to record the pulse streams. This oscilloscope has an extended acquisition mode that allows the recording of 8 million points. Thus half of this available storage capacity was used to record synchronous PPM trigger on one of the oscilloscope channels while the remaining half was used to store the APD output. Typical sampling rates used were 500 MS/sec and 1 GS/sec. Thus the maximum number of pulses that could be recorded were 400 or 800. Matlab routines have been developed for performing spot checks on the number of pulses received using a maximum likelihood algorithm. The output of the maximum likelihood algorithm can be compared with the recorded trigger pulses where the laser is known to have fired in order to obtain symbol and bit error rates.

3. COMPARISON OF RESULTS WITH THEORY

Laboratory APD performance is evaluated through comparisons of the APD output statistics and PPM bit error probabilities with analytical probability density functions and error rate calculations. In order for the laboratory performance to match theoretical predictions, it is important that the statistical characteristics of the empirical data match the theoretical models. If the probability distributions of the APD output statistics for signal and noise (non-signal) slots in the empirical data match the theoretical probability density functions well, we can be confident in basing system designs on the theoretical models. We provide a number of plots that compare the empirically constructed distributions of signal and non-signal slots to those predicted by theoretical analysis and approximation, and we compare the experimental and theoretical bit error rates for a detection algorithm under the assumption of perfect time synchronization.

3.1. Analytical Model of the APD Channel

Following the formulation found in [4], we model the output of the APD photodetector package as the sum of Webb and Gaussian random variables. The average number of photons absorbed by an APD illuminated with total optical intensity $\lambda(t)$ in T_s seconds can be expressed as

$$\bar{n} = \frac{\eta}{h\nu} \int_0^{T_s} \lambda(t) dt \tag{1}$$

where h is Planck's constant, ν is the optical frequency, and η is the detector's quantum efficiency, defined as the ratio of absorbed to incident photons. The actual number of photons absorbed, n, is a Poisson distributed random variable. The probability $p(m|\bar{n})$ that an APD generates m output electrons given $\bar{n}$ mean absorbed photons can be derived from the McIntyre-Conradi distribution [7], but may be approximated by the continuous Webb density function [8] as follows:

$$p(m|\bar{n}) = \frac{1}{\sqrt{2\pi\bar{n}G^2F}\left(1+\frac{m-G\bar{n}}{\bar{n}GF/(F-1)}\right)^{3/2}} \exp\left(-\frac{(m-G\bar{n})^2}{2\bar{n}G^2F\left(1+\frac{m-G\bar{n}}{\bar{n}GF/(F-1)}\right)}\right). \tag{2}$$

Here, G is the average APD gain, k is the ionization ratio, and F is the excess noise factor given by $F = kG + (2 - 1/G)(1-k)$. Added to the random number of APD output electrons is an independent Gaussian thermal noise charge from the follow-on electronics [4]. The probability density function for the slot statistic is therefore the convolution of the Webb and Gaussian density functions, and may be written as

$$p(x|\bar{n}) = \sum_{m=0}^{\infty} \phi(x, \mu_m, \sigma^2) p_w(m|\bar{n}), \tag{3}$$

where $\phi(x, \mu_m, \sigma^2)$ is the Gaussian density function with mean $\mu_m = mq + I_s T_s$ and variance $\sigma^2 = \left(2qI_s + \frac{4\kappa T}{R}\right) BT_s^2$, as given in [4]. Here, q is the electron charge, κ is Boltzmann's constant, T is the equivalent noise temperature, I_s is the APD surface leakage current, and B is the single-sided noise bandwidth. The value of the load resistance R_L

Table 1. System parameters for APD channel.

Parameter	532 nm APD	1064 nm APD
M (PPM order)	256	256
T_s (PPM slot duration)	25 ns	10 ns
η (quantum efficiency)	0.8	0.38
k (ionization ratio)	0.0015	0.02
G (average gain)	150	19
I_s (surface leakage current)	4.2 nA	100 nA
I_b (bulk leakage current)	42 pA	10 pA
T (equivalent noise temperature)	1993 K	300 K
R_L (load resistance)	10 kΩ	1.5 kΩ

is given by the feedback resistance of the transimpedance amplifier following the APD. Note that the APD surface leakage current is not multiplied by the APD gain and is modeled here as a constant DC current. The bulk dark current I_b, on the other hand, is multiplied by the APD gain and is modeled as part of the background radiation.

An approach that is commonly used to simplify calculation of PPM symbol error probabilities is to model the density of the APD output electron charge as Gaussian with mean $qG\bar{n}$ and variance $q^2G^2F\bar{n}$. Then the slot statistic consisting of the sum of APD output electrons and amplifier thermal noise is also Gaussian, and has mean $\mu = qG\bar{n} + I_sT_s$ and variance $\sigma^2 = \left[2q^2G^2F\bar{n} + qI_sT_s + \frac{4\kappa TT_s}{R_L}\right] BT_s$. Although simple, this approximation does not yield accurate results over all regions of interest, as previously shown in [4].

For M-ary PPM with slot duration T_s, the total charge is integrated over each slot time T_s, resulting in a vector of M independent observables for each received PPM word. It was shown in [9] that given these observables, the maximum likelihood detector structure consists of choosing the PPM symbol corresponding to the slot with the largest accumulated charge value. If $\bar{n}_b$ and $\bar{n}_s$ are the mean number of absorbed background photons per slot and the mean number of absorbed signal photons per pulse, respectively, the M-ary PPM symbol error probability is

$$P_e(M) = 1 - \int_{-\infty}^{\infty} p(x|\bar{n}_b + \bar{n}_s) \left[\int_{-\infty}^{x} p(y|\bar{n}_b)dy\right]^{M-1} dx, \tag{4}$$

where $p(x|\bar{n})$ is given in (3).

3.2. Probability density function comparisons

Output voltage signals from the 532 nm APD and 1064 nm APD were sampled at a rate of 500 megasamples per second and accumulated to form 25 nanosecond slots, with 12.5 samples per slot. These slots were then separated into signal and non-signal (noise) slots. Note that these slot statistics are in units of accumulated voltage over a slot, whereas the analytical model of the previous subsection was presented in terms of accumulated slot charge. In the plots the charge is simply converted to voltage across the load resistor by multiplying by qR_L/T_{sample}, where T_{sample} is the sample time.

The slot counts can be put into a histogram in order to show the empirical probability density function (pdf). Due to the high order of PPM signaling used and the amount of dead time between PPM words (50 kHz repetition rate for the 532 nm APD and 100 kHz repetition rate for the 1064 nm APD), as simply a set of additional noise slots, there are significantly more noise slots than signal slots. More specifically, for the 532 nm APD there were 400 signal slots and over 300,000 noise slots, and for the 1064 nm APD there were 800 signal slots and over 700,000 signal slots. This means that the empirically observed noise slot pdf should be quite close to the actual pdf, while the empirical signal pdf may exhibit more unevenness.

The parameters required to predict the pdf's of the APD outputs are given in Table 1. The noise equivalent bandwidth is approximated to be $B = 1/(2T_s)$ Hz, which is that of an ideal integrator over duration T_s. Although the equivalent noise temperature was estimated for the 532 nm APD by tuning the gain to nearly zero and measuring

the noise power output of the preamplifier, this measurement was unable to be taken for the 1064 nm APD so room temperature was used as a default.

Using these parameters, the pdf's for the Webb+Gaussian model of the APD were computed for each collection run. The density function requires computation of a convolution integral for each point on the curve. A comparison of the empirical and theoretical pdf's are shown in Figs. 2-5 for the two APD when there are zero and 100 incident background photons ($\bar{n}_{bi}$) per slot. In each figure, plots of the lowest signal power and highest signal power in the data collection run are shown. There was DC bias that varied with the background power, so in all of the figures the empirical curves were shifted so that the empirical noise pdf peak lined up with the theoretical noise pdf peak. The separation between signal and noise, however, is the feature that predicts error performance.

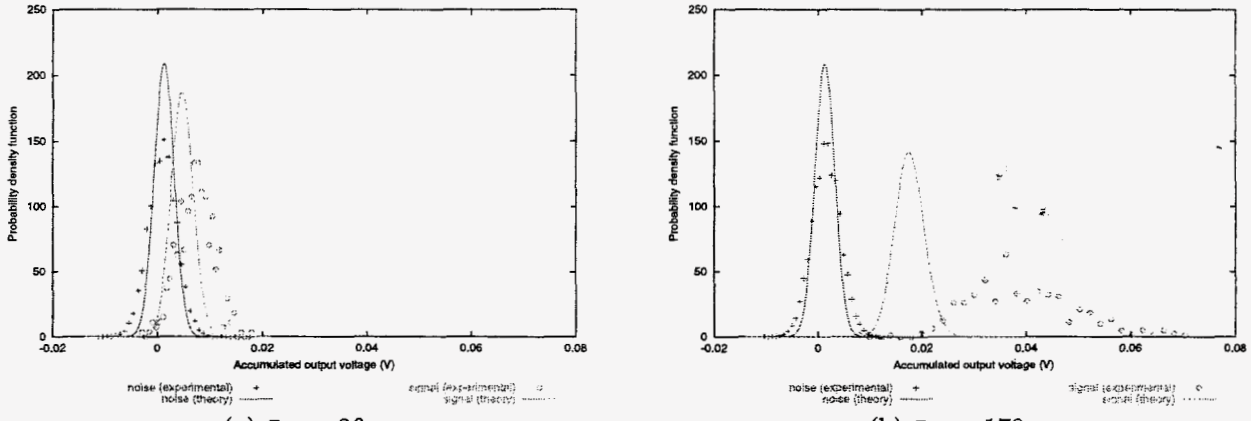

(a) $\bar{n}_{si} = 36$ (b) $\bar{n}_{si} = 170$

Figure 2. Comparison of empirical and theoretical pdf's, 532 nm APD, $\bar{n}_{bi} = 0$.

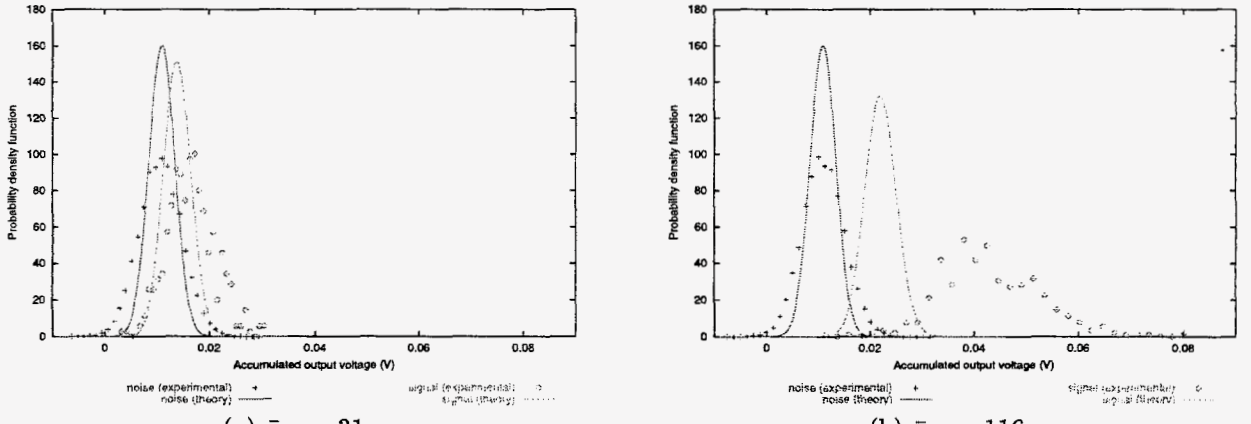

(a) $\bar{n}_{si} = 31$ (b) $\bar{n}_{si} = 116$

Figure 3. Comparison of empirical and theoretical pdf's, 532 nm APD, $\bar{n}_{bi} = 100$.

As may be seen in Figs. 2 and 3, there are significant discrepancies between the empirical and theoretical pdf's for the 532 nm APD data. Note that the empirical noise pdf's are smooth and fairly Gaussian in appearance, while the empirical signal pdf's are more irregular, due to the small sample size of the signal slots. All of the plots show that the variances of both the empirical noise and empirical signal distributions are larger than the theoretical values. In addition, the separation between the empirical noise and signal distributions is larger than that between the theoretical curves, a feature more evident the the higher power plots of Fig. 2(b) and Fig. 3(b).

We continue to believe that the Webb+Gaussian model is the best model to use to design a communications link. It is most likely that the main cause of discrepancies between the empirical and theoretical results is inaccurate estimation of parameters, which can dramatically affect the theoretically predicted results. This may include imprecise

knowledge of the APD gain, system noise temperature, and received signal and background levels, as well as timing jitter in the laser and unknown causes of DC bias.

In roughly what we believe to be the order of significance regarding the causes of the discrepancies, we consider these parameters. First, the gain of the APD was derived from using DC white light illumination as provided by the manufacturer. Since this may lead to discrepancies when pulsed light is used, more accurate gain measurement techniques are being investigated. Although the effective noise temperature of the preamplifier load was measured at 1993 K when the APD gain was made very small, it appears from Figs. 2 and 3 that T may be even higher. Mis-estimation of system noise temperature would help explain discrepancies observed in the variances of both the signal and noise slot counts. Another possible explanation for the discrepancies is imperfect modeling of the laser power. For most data runs, the separation between the non-signal and signal pdf's was greater than predicted. This is consistent with an underestimate of the actual mean number of photons reaching the APD detector. We do not believe that timing jitter has a large effect on the results for the 532 nm APD. Primarily, this is because the timing jitter was mostly confined to within a few nanoseconds, and the pulse itself was only a small fraction of the 25 ns slot duration, so that the pulse may vary by perhaps up to even 10 ns in either direction without falling outside of the slot boundary. Finally, quantization error due to the 8-bit quantization of the recording digital oscilloscope may degrade the accuracy of the data, but does not explain the systematic differences we observe in the pdf's.

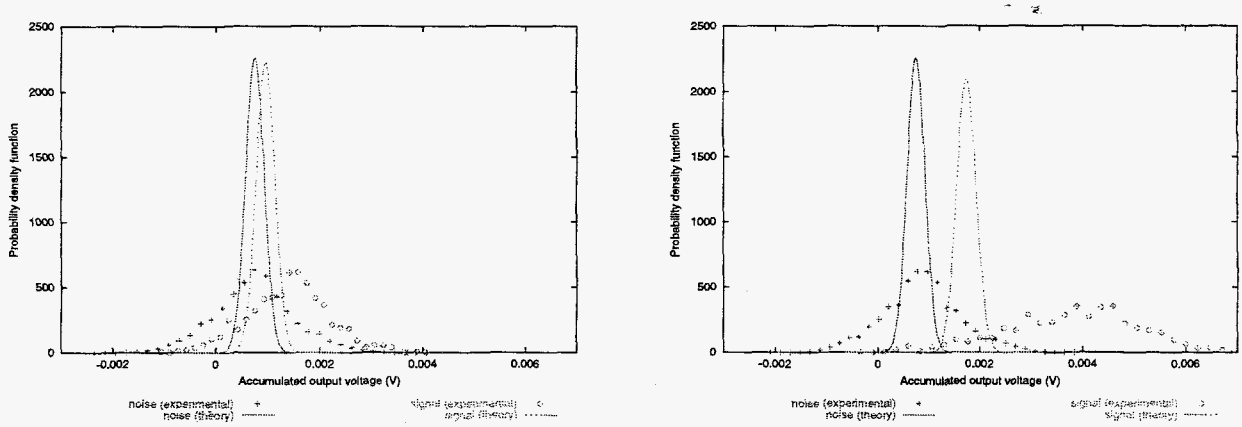

(a) $\bar{n}_{si} = 235$ (b) $\bar{n}_{si} = 1142$

Figure 4. Comparison of empirical and theoretical pdf's, 1064 nm APD, $\bar{n}_{bi} = 0$.

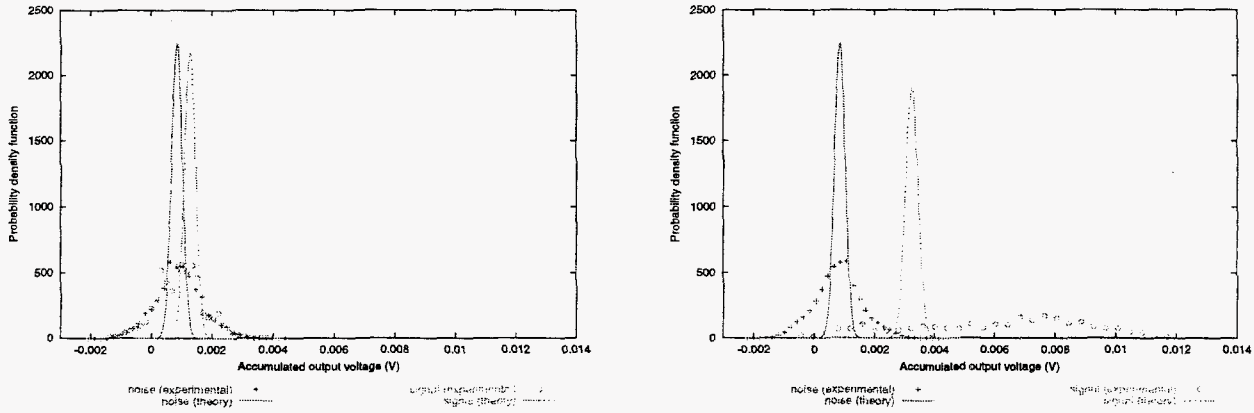

(a) $\bar{n}_{si} = 496$ (b) $\bar{n}_{si} = 2766$

Figure 5. Comparison of empirical and theoretical pdf's, 1064 nm APD, $\bar{n}_{bi} = 100$.

There are several parametric differences between the 532 nm detector and the 1064 nm detector, as shown in Table 1. The longer wavelength detector has half the quantum efficiency of the 532 nm APD, as well as a much lower average gain value and higher ionization ratio. The mismatch between laboratory results and theory is even

more pronounced for the 1064 nm APD. For this detector, we were able to collect twice as many signal samples (the pulse repetition rate was twice that for the 532 nm APD data), so the empirical signal pdf's are somewhat smoother than those in Figs. 2 and 3. However, we observe that the mean and variance discrepancies continue to be large for this detector, for many of the same reasons as for the 532 nm detector. Once again, the gain value used was manufacturer-provided, and may not be accurate. More significantly, due to the inability to tune the gain for this APD, we were unable to make a noise temperature measurement. The default room temperature value of 300 K is obviously too low. Although a higher noise temperature would result in a larger variance, it would not explain the large discrepancy between the empirical and theoretical signal means, especially in the higher signal photon cases. Finally, the narrower slots (10 ns) used for this detector may also affect the empirical pdf's, since timing jitter would be more likely to cause the signal pulse to slip out of the signal slot, thereby corrupting the histogram data collection.

4. BIT ERROR RATE COMPARISONS

The slot counts collected to create the empirical pdf's may also be used to calculate the empirical uncoded symbol error rate (SER), by comparing each signal slot count with 255 non-signal slot counts. The theoretical uncoded SER is calculated using (4), with both the Webb+Gaussian as well as the slightly less accurate completely Gaussian approximation used for the APD output density function. The uncoded symbol error rate is converted to an uncoded bit error rate (BER) via the approximation

$$BER \approx \frac{M(SER)}{2(M-1)}, \tag{5}$$

where $M = 256$ is the PPM order. A comparison of the empirical and theoretical BER's are shown in Figs. 6 and 7 for the 532 nm and 1064 nm detector data, respectively. Because only 400 or 800 symbols were processed for each empirical BER point, we also computed the 95% confidence interval based on sampling from a binomial distribution.

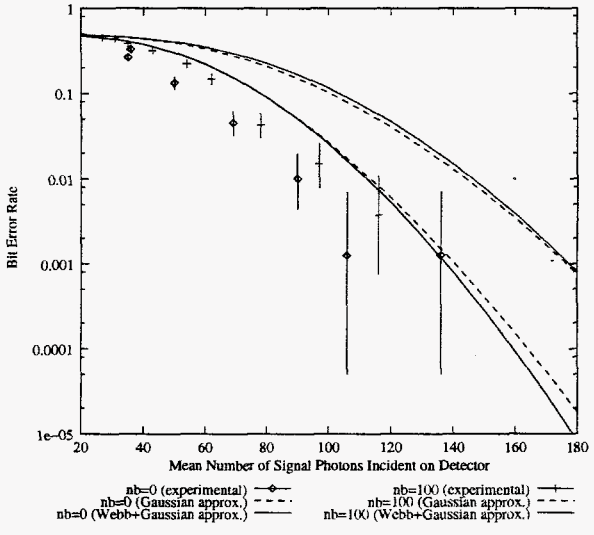

Figure 6. Comparison of empirical and theoretical bit error rates, 532 nm APD, $\bar{n}_{bi} = 0$ and $\bar{n}_{bi} = 100$.

The bit error rates shown in Figs. 6 and 7 are consistent with the pdf's shown earlier. In Figs. 2 and 3, the empirical separation between the noise and signal pdf's is larger than theoretically predicted for the 532 nm APD. This is also reflected in the BER's of Fig. 6, which show an empirical BER 1 to 2 dB lower than predicted with either a Gaussian model or a Webb+Gaussian model. Note that at lower error probabilities, the error bars are quite large due to the lack of an adequate sample size. On the other hand, the empirical bit error rates for the 1064 nm APD are larger than theoretically predicted by more than 1.5 dB, and appear to approach a floor. Although, as shown in Figs. 4 and 5, the empirical separation between noise and signal pdf's is once again larger than expected, the empirical variance is also much larger than the theoretical variance, leading to a higher error probability. It is also worth noting that the two background cases shown here, $\bar{n}_{bi} = 0$ and $\bar{n}_{bi} = 100$, have practically identical theoretical BER curves. The cause of the "tailing off" of the empirical BER could be timing jitter that causes errors regardless of how high the signal photon count is made.

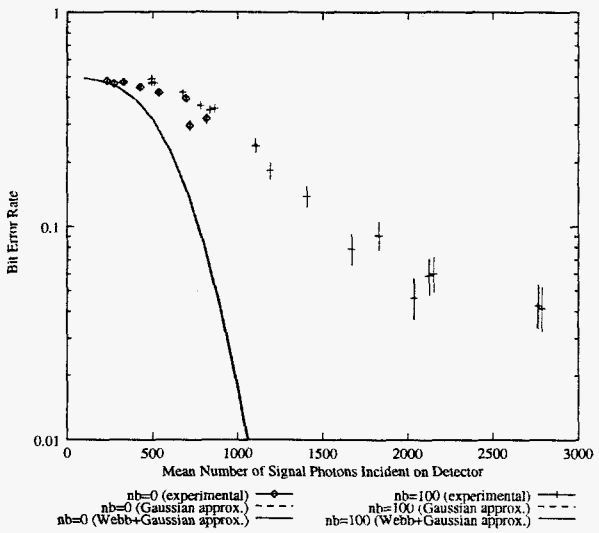

Figure 7. Comparison of empirical and theoretical bit error rates, 1064 nm APD, $\bar{n}_{bi} = 0$ and $\bar{n}_{bi} = 100$.

5. CONCLUSIONS

In this paper, the results of experiments using commercially available silicon avalanche photodiodes for pulse position modulation detection were compared with theoretical models in order to characterize the real-world performance of these detectors. Both a 532 nm and a 1064 nm APD were tested through the construction of empirical probability density functions for signal and noise PPM slots, and through the calculation of bit error probabilities. Although there is some qualitative agreement between the experimental results and theory, significant discrepancies exist between the means and variances of the output statistics, which are reflected in the bit error rates. Many of these discrepancies may be traced to imprecise knowledge of channel parameters, especially noise equivalent temperature and average APD gain. It is crucial that these discrepancies be examined and understood in order to enable the design of mission link budgets and develop optical receiver processing hardware. Continuing work will focus upon resolving the discrepancies and closing the gap between theory and practice.

REFERENCES

1. T.-Y. Yan and C.-C. Chen, "Design and development of a baseline deep space optical PPM transceiver," in *Proceedings of SPIE, Free-Space Laser Communications Technologies XI*, G. S. Mecherle, ed., vol. 3615, pp. 154–169, 1999.
2. C.-C. Chen, "Figure of merit for direct-detection optical channels," *JPL Telecommunications and Data Acquisition Progress Report* **42-109**, May 1992.
3. G. G. Ortiz, J. V. Sandusky, and A. Biswas, "Design of an opto-electronic receiver for deep-space optical communications," *JPL Telecommunications Mission Operations Progress Report* **42-142**, August 2000.
4. F. M. Davidson and X. Sun, "Gaussian approximation versus nearly exact performance analysis of optical communications systems with PPM signaling and APD receivers," *IEEE Transactions on Communications* **COM-36**, pp. 1185–1192, November 1988.
5. G. L. Unger, M. A. Krainak, and X. Sun, "Comparison of direct 50 mbps q-ppm receiver performance for algaas and nd doped laser transmitters," in *Proceedings of SPIE Free-Space Laser Communciations Technologies IV*, vol. 1635, 2, 1992.
6. H. Plaessmann, K. S. Yamada, C. E. Rich, and W. M. Grossman, "Sub-nanosecond pulse generation from diode pumped acousto-optically q-switched solid-state lasers," *Applied Optics* **32**, pp. 6616–6619, 1993.
7. R. J. McIntyre, "The distribution of gains in uniformly multiplying avalanche photodiodes: Theory," *IEEE Transactions on Electron Devices* **ED-19**, pp. 703–713, June 1972.
8. P. P. Webb, R. J. McIntyre, and J. Conradi, "Properties of avalanche photodiodes," *RCA Review* **35**, pp. 234–278, June 1974.
9. V. Vilnrotter, M. Simon, and M. Srinivasan, "Maximum likelihood detection of PPM signals governed by an arbitrary point process plus additive gaussian noise," *Electronics Letters* **35**, July 1999.